May 2002

Sensor based door navigation for a nonholonomic vehicle

Sarangi Patel
University of Pennsylvania

Sang-Hack Jung
University of Pennsylvania

James P. Ostrowski
University of Pennsylvania

Rahul Rao
University of Pennsylvania

Camillo J. Taylor
University of Pennsylvania, cjtaylor@cis.upenn.edu

Copyright 2002 IEEE. Reprinted from *Proceedings of the 2002 IEEE International Conference on Robotics and Automation (ICRA 2002)*, Volume 3, pages 3081-3086.
Publisher URL: http://ieeexplore.ieee.org/xpl/tocresult.jsp?isNumber=21827&page=9

Sensor based door navigation for a nonholonomic vehicle

Abstract
This paper presents a sensor based algorithm for guiding a nonholonomic platform, such as a wheelchair, through a doorway. The controller uses information from a camera system and a laser range finder to perform image-based navigation. Simulations of the resultant switching controller are presented along with experimental results. A simple obstacle avoidance algorithm is also implemented on the experimental platform. Finally, we have considered the input of limited field-of-view constraints on this controller. All of these components together lead to a modal, image-based approach that will safely and robustly navigate a nonholonomic robot with sensor constraints through a doorway.

Keywords
computer vision, laser ranging, navigation, sensor fusion, image-based approach, image-based navigation, laser range finder, nonholonomic vehicle, obstacle avoidance algorithm, sensor based door navigation, sensor constraints, switching controller, wheelchair

Proceedings of the 2002 IEEE
International Conference on Robotics & Automation
Washington, DC • May 2002

Sensor based door navigation for a nonholonomic vehicle

Sarangi Patel*, Sang-Hack Jung†, James P. Ostrowski*, Rahul Rao*, and Camillo J. Taylor†
*Mechanical Engineering and Applied Mechanics, †Computer and Information Science
GRASP Laboratory, University of Pennsylvania
{sarangi,sangj,jpo,rahulrao,cjtaylor}@grasp.cis.upenn.edu

Abstract

This paper presents a sensor based algorithm for guiding a nonholonomic platform, such as a wheelchair, through a doorway. The controller uses information from a camera system and a laser range finder to perform image-based navigation. Simulations of the resultant switching controller are presented along with experimental results. A simple obstacle avoidance algorithm is also implemented on the experimental platform. Finally, we have considered the input of limited field-of-view constraints on this controller. All of these components together lead to a modal, image-based approach that will safely and robustly navigate a nonholonomic robot with sensor constraints through a doorway.

1 Introduction

There has been significant recent interest in harnessing the power, precision, and flexibility of robots to augment the abilities of human users. We describe an approach to enhancing the capabilities of one of the most commonly used assistive devices, the motorized wheelchair. At present, motorized wheelchairs still require fairly precise low level control inputs from the user. Unfortunately, many users who could benefit from motorized wheelchairs lack these fine motor skills. For instance, those with cerebral palsy may not be able to guide a chair through a narrow opening, such as a doorway, without bumping into the sides numerous times. By outfitting the wheelchair with a control system, a camera and a laser range finder, we are able to provide the user with a high level interface to low level controllers that safely guides our smart wheelchair through constricted passages.

In our approach to this problem, we take explicit advantage of the user's ability to make decisions regarding the destination. The user is presented with an image of the surroundings in which he can select the opening that the robot should traverse. The system then automatically guides the platform through the specified doorway.

Our control algorithms are based on visual servoing techniques. Hutchinson, Hager and Corke [1] provide a thorough explanation of visual servo control. Visual servoing is divided into two broad categories– *image-based* servoing [2, 3], in which the control inputs are derived directly from the sensor measurements, and *pose-based* servoing [4], where the pose of the robot is reconstructed in order to determine the control inputs. There has also been some limited, but interesting, work done on visual servoing for nonholonomic robots [5, 6]. In particular, Ma et al. [5] propagate the nonholonomic constraints into the image plane and show that standard controllers for nonholonomic systems can be applied. We utilize some similar ideas, but attempt to extend the results to include the effect of sensor constraints.

There are also several papers that we would like to bring to attention since they are closely related to our work. Cowan and Koditschek [3] have done work on planar image-based servoing with the added constraint of keeping feature points in view. Our work parallels this direction of research; however, we are also concerned with incorporating nonholonomic constraints that arise when working with wheeled vehicles. Since we are traversing doorways, we are able to use some innate doorway characteristics. For example, we assume the sides of the doorway are parallel to each other and they can be projected on the image plane [7, 8]. Of particular relevance, however, is the work by Eberst et al. [9] who have presented vision-based doorway navigation for an omnidirectional robot. They have used a reconstruction approach while we use an image-based approach. Our work further contributes to doorway navigation by specifying control algorithms that successfully and efficiently drive the system through the doorway in the presence of sensor and nonholonomic constraints.

2 The Experimental Platform

2.1 The Wheelchair

We have outfitted a motorized wheelchair with onboard processing and a suite of sensors as seen in Figure 1. The omni-directional camera, mounted over the user's head, allows the user to view 360 degrees around the wheelchair. The projector system displays images onto the laptray and enables the user to send commands to the wheelchair through a visual interface. The laser

0-7803-7272-7/02/$17.00 © 2002 IEEE

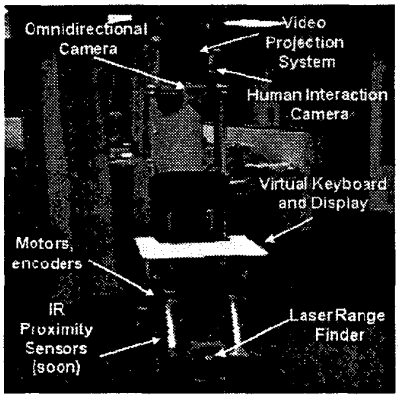

Figure 1: The wheelchair setup

scanner, mounted between the feet, measures distances over a 180 degree range.

2.2 System Model

In order to analyze the system and develop controllers, we place an inertial coordinate frame at the center of the doorway (see Figure 2). This coordinate frame is slightly unintuitive, but has the advantage that the goal position is the origin, $(x, y, \theta) = (0, 0, 0)$.

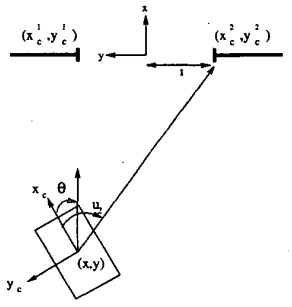

Figure 2: Coordinate frames of the system.

The model for our system is a two-wheeled, nonholonomic cart-like robot, with position referenced by the center of the two wheels. The governing equations for the wheelchair are well-known [5]:

$$\begin{aligned} \dot{x} &= v\cos(\theta) \\ \dot{y} &= v\sin(\theta) \\ \dot{\theta} &= \omega, \end{aligned} \tag{1}$$

where the inputs are the forward velocity, v, and angular velocity, ω.

In servoing to doors, we characterize doorways as having two strong vertical lines in the image plane. For a camera mounted on a planar robot, this implies that each feature (vertical line) can be though of as having a projection to a single point in the image space. Thus, a vertical line can be described by its coordinates in the inertial frame, say (x_f, y_f). If we denote by u the azimuth angle to which the vertical line is projected in the image plane, and write the location of the line in terms of a camera coordinate frame (coinciding with the body reference frame of the robot), $(x_c, y_c), u = \text{atan2}(y_c, x_c)$, where

$$\begin{pmatrix} x_c \\ y_c \end{pmatrix} = \begin{pmatrix} \cos\theta & \sin\theta \\ -\sin\theta & \cos\theta \end{pmatrix} \begin{pmatrix} x_f - x \\ y_f - y \end{pmatrix},$$

and (x, y, θ) describes the robot's current pose in the inertial frame.

If we denote the locations of the door edges to be at $(0, \pm l)$, then the two edges will project to

$$u_1 = \tan^{-1}\left(\frac{x\sin\theta + (l-y)\cos\theta}{-x\cos\theta + (l-y)\sin\theta}\right), \tag{2}$$

$$u_2 = \tan^{-1}\left(\frac{x\sin\theta - (l+y)\cos\theta}{-x\cos\theta - (l+y)\sin\theta}\right), \tag{3}$$

where u_1 denotes the left door edge, and u_2 the right. With this information alone, we cannot determine the inertial position of the robot. However, merging this data with the laser range data, we are able to extract a pose for pose-based servoing.

3 Pose Estimation and Prediction

Sensor measurements from three different modalities are fused to produce a unique representation of the target. The omnidirectional camera is aligned with the laser scanner. The physical offset between the two sensors is used to form a transformation function which maps depth and azimuth angle estimates from the laser to the corresponding azimuth angle on the image.

The odometry is used to predict the target position with respect to the inertial coordinate system during navigation. The robot position is then updated to minimize the prediction error using the relative position estimates from the vision and laser sensors. In order to make the feature tracker more robust, we have explored a gradient update method for the pose estimates derived from the Sick laser data.

The vision system collects 360 degree view images and unwarps them into panoramic images where the vertical lines are preserved. The target vertical lines marked by the user on the initial state (drawn as two boxes on the unwarped image in Figure 3) are tracked to give the target's relative azimuth position.

The vertical line extraction from vision, along with odometric predictions, are used to guide the initial search of the depth map to find discontinuities characteristic of

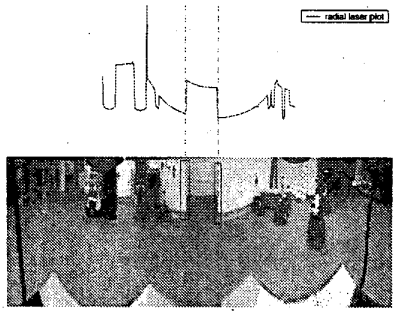

Figure 3: Laser (top) and unwarped image (bottom) matching.

a doorway. This is shown in Figure 3, where the dashed vertical lines show the matching of the image and laser data. The azimuth value of these discontinuities is coupled with depth to update the estimate of target position, and is correlated with the estimates from the vision in order to reject bad data.

Each estimate calculated from the sensors is updated with odometry. The relative position estimate is used to predict and update the target position.

4 Controllers

A wide variety of possible methods for controlling such a system exist (see e.g., work by Canudas de Wit and Sordalen [10]). Topological restrictions (often referred to as Brockett's necessary condition) place certain limits on the achievable tasks using smooth, static state feedback. For this reason, we generally pursued controllers that did not seek to stabilize to the origin, but rather whose goal was to drive the robot through the center of the doorway by converging to the x-axis defined by the doorway (see Figure 2). Additionally, we explored the use of image-based switched controllers, since these have the potential to provide better overall performance.

4.1 Image-based, Switching Controller

Instead of relying on a simple pose-based controller to do the servoing, we explored the potential of an image-based controller that did not rely so severely on depth[1]. This controller uses two basic types of feedback modes: one attempts to maintain one of the features in a fixed location, usually at or near the boundary of the sensor, and the other relies on centering the robot between the two features. Thus, the first controller is used to steer the robot towards (and through) the middle of the doorway, while the second is used to drive the robot through the doorway.

[1] In fact, although this image-based controller uses depth in the Jacobian estimates, this requirement can be completely removed with only a small loss in performance

In order to explore these two controllers in more detail, we look at the effect of the controllers on the motion of the features in the image plane. Using the projective model given in Eqs. 2 and 3, combined with the equations of motion for the robot (Eq. 1), we find (after some interesting algebraic simplifications) that the equations governing the motion of the features, (u_1, u_2) are

$$\dot{u}_1 = -\omega + \frac{v}{z_1}\sin u_1 \tag{4}$$

$$\dot{u}_2 = -\omega + \frac{v}{z_2}\sin u_2, \tag{5}$$

where z_1 is the distance from the camera to the vertical line being tracked, given by

$$z_1^2 = x^2 + (l - y)^2$$

(and respectively, $z_2^2 = x^2 + (l + y)^2$). The two proposed controllers derive directly from Eqs. 4 and 5 and are discussed individually in the next two sections.

4.1.1 Sensor Constraint Controller

Although our use of an omnicam gives us a 360° field-of-view, we have developed this controller to be used also for traditional, narrow field-of-view, perspective projection cameras.

We choose a desired maximum heading angle, $u_{\max}$, where we wish to view the features (i.e., we constrain the features to satisfy $-u_{\max} < u < u_{\max}$). This heading angle is also used to help with the steering. We formulate this motion as a regulation problem, where one of the two features (vertical lines) is kept at its maximum allowable viewing angle, $u_{\max}$. This is dependent on the initial location of the robot— if we start to the left of the door ($y > 0$), we usually want to keep the left-most feature (u_1) on the edge of our sensing. Alternatively, if we start on the right side of the door ($y < 0$), we keep the right-most feature (u_2) on the boundary. For example, if the robot is initially on the left side, then we seek a controller that drives u_1 to $u_{\max}$. We generally have chosen $v = v_{\max}$ to be a constant velocity, so our controller becomes:

$$\omega = K_1(u_1 - u_{\max}) + \frac{v}{z_1}\sin u_1,$$

which leads to exponential convergence to the desired value of $u_{\max}$. Even with very crude estimates of depth, z_i, the convergence properties are very good.

4.1.2 Centering Controller

A controller that keeps the center of the doorway in front of the robot is appealing. In practice, however, this can only be applied when the robot is roughly in front of the

doorway; otherwise, the robot may try to cut through to the doorway at too sharp an angle. For this reason, we utilize this type of controller only after the robot has been brought within a certain threshold of the center of the doorway.

For simplicity the goal is to keep the robot heading centered between the two image features, rather than the actual center of the doorway. This incurs some small errors in the final location of the robot as it crosses the doorway, but these are not significant. It should also be mentioned that this controller no longer maintains sensor constraints, since it is not possible to satisfy sensor constraints while moving through a doorway with less than a 180° field-of-view.

Our controller is designed to regulate the average value, $\frac{1}{2}(u_1 + u_2)$, to zero. Given the velocity, v, an exponentially converging controller is

$$\omega = K_{12}\left(\frac{u_1 + u_2}{2}\right) + v\left(\frac{\sin u_1}{z_1} + \frac{\sin u_2}{z_2}\right).$$

The switching controller works quite well in simulation, and in practice.

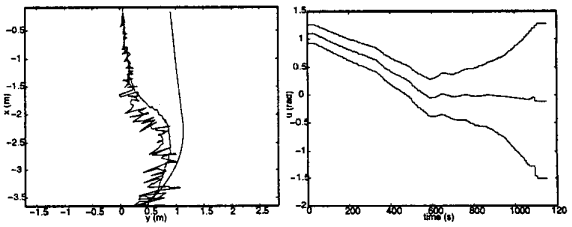

Figure 4: Experiment using a switched controller

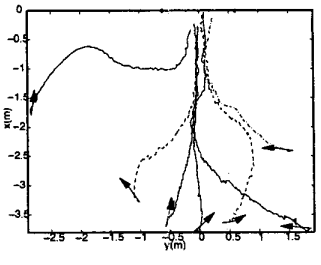

Figure 5: Results for several experimental trials

4.1.3 Experimental Results

Figure 4 shows results for the experiment. The left plot shows the (x, y) position, both given through odometry estimates (dashed curve) and for estimates based on the combined image and laser data (jagged curve). It also shows the curve produced when the data from the different sensors is combined. Note that the pose estimates from the laser and vision data alone, even if outliers were to be removed, are very noisy and were found to be unsuitable for controlling the robot. Odometry estimates also cannot be relied on directly since the drift due to the heading error, although small, is unacceptable. Thus, the gradient method proves to be successful in incorporating the raw data into information that will allow the wheelchair to proceed through the doorway. The key is to properly mix the relative pose information from odometry with the noisy absolute pose data from the laser. The right plot shows the image features (u_1, u_2) and their center value. In Figure 5, we plot the results of our pose estimates from a few runs, all of which were successful at navigating the doorway.

4.2 Regions of Attraction

The switching controller is further examined by taking a closer look at the area around the doorway. Figure 6 illustrates the segmented regions of the surrounding area. The location of the chair determines the control mode that gets selected. Region I is the *centering region*. If the wheelchair is initially in this region, then it will not have to switch to another control mode to pass through the doorway. If the wheelchair begins in Region II, then it will be forced to switch modes from the sensor constraint controller to the centering controller. Any initial position in Region III cannot be guaranteed to go through the doorway. Another way to descibe this is by defining the goal as G and the domain of attraction as D. Thus, for the first controller, $\Phi_{\mathrm{I}} : D(\Phi_I) \longrightarrow G(\Phi_I)$. In this case, the domain of attraction, $D(\Phi_I)$, is Region I, while the goal of the controller, $G(\Phi_I)$, is motion through the doorway, given by $\{x = 0, y \in [-l + \frac{w}{2}, l - \frac{w}{2}]\}$. For the second controller, $\Phi_{\mathrm{II}} : D(\Phi_{II}) \longrightarrow G(\Phi_{II})$. To connect these controllers we observe that $G(\Phi_{II}) \subset D(\Phi_I)$. That is, in the language of Koditschek et al. [3], Φ_{II} *prepares* Φ_I, or $\Phi_{\mathrm{II}} \succeq \Phi_{\mathrm{I}}$. This means that when the chair is located in Region II, it will be attracted to Region I, whose domain of attraction is the doorway.

Boundaries of these regions have been derived by:

$$\dot{r} = -v\cos\phi \tag{6}$$

$$\dot{\theta} = \frac{v}{r}\sin\phi \tag{7}$$

$$\frac{dr}{d\theta} = -r\cot\phi \tag{8}$$

where (r, θ) are in polar coordinates with respect to a coordinate system placed at the one edge of the doorway. Solving this differential equation gives:

$$r(\theta) = -r_o e^{-\theta\cot\phi}. \tag{9}$$

The total path length, L, is found to be $L = r_o \sec\phi$. After substitutions and algebraic manipulations, we find

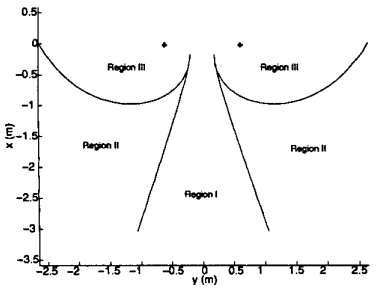

Figure 6: Control mode regions

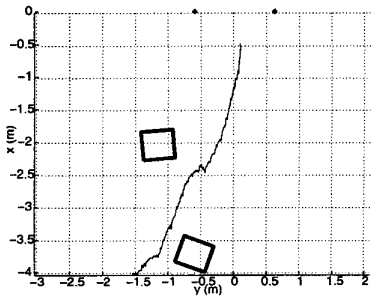

Figure 7: Experimental trial of obstacle avoidance

the following:

$$r(t) = r_o - vt\cos\phi \tag{10}$$

where v is our constant forward velocity. By solving Eq. 9, we get:

$$\theta(t) = \ln[\frac{r_o}{r}]\tan\phi. \tag{11}$$

Thus, $r(t)$ and $\theta(t)$ describe the position of the robot at every time step and help define the boundaries of the various regions.

4.3 Obstacle Avoidance

We have implemented a simple obstacle avoidance algorithm on our platform. If obstacles are detected within the specified minimum distance around the wheelchair, the obstacle avoidance algorithm is activated. The detection of objects is done by the laser scanner which continuously provides distance feedback of objects in its range. When the obstacle avoidance algorithm is activated, the chair smoothly avoids the obstacle by going around it while also continuing towards the doorway destination.

During obstacle avoidance, the robot is guided by the new direction, which is the sum of the original heading direction from the controller and the repulsive direction from the obstacle. Thus, the chair does not go off course when an obstacle appears, but rather, the control algorithm is able to correct the disturbance by proceeding to minimize the distance between the wheelchair and its final goal. Although we have yet to prove completeness conclusively, we believe that this will be the case under certain basic assumptions about the initial configuration and the free path leading to the doorway. Of course if both edges are obstructed or there isn't enough space for the wheelchair to get through, it will not be able to continue. However, in cases where an edge is visible and there is enough space, the wheelchair is able to navigate through the doorway. See Figure 7.

4.4 Narrow Field-of-view Limitations

Any nonholonomically constrained mobile system that must work with field-of-view constraints cannot pass through the doorway while maintaining only a forward velocity. Thus, this section describes what to do when the wheelchair is in Region III. If the robot starts in Region II, the controller will generally drive the robot into the "centering" region (Region I), where the second controller takes over. If the robot starts in Region III, before entering Region I, the controller will drive the robot so that the second image feature will move to its limiting value as the robot gets too close to both features.

To handle this scenario, we have made an additional modification to the controller when it is in Region III (where one feature is kept on the boundary of the sensor constraint). When the system drives to a limiting point where both features are at their maximum (boundary) values, the controller switches to tracking the secondary feature to remain on the boundary, and moves in reverse.

This motion is guaranteed to eventually drive the robot to Region I. However, it may require moving very far away from the initial target, which is not practical. For this reason, we add an additional switching condition whereby the controller switches back to the original feature tracking if the robot moves further away than its original distance from the target.

A simulation of this behavior is shown in Figure 8 for a camera with a 50° field of view. Notice that the motion of the robot (shown in the left plot) resembles a parallel parking maneuver. This is characteristic of this type of switching— in the process, it both satisfies the sensor constraints and maintains a reasonable distance to the target. We believe, though have not yet been able to show, that this is the best controller to use when the features must stay within certain constraint limits. The justification for this is that this controller always acts at the limits of its sensor space (i.e., it is a "bang-bang" type controller).

The motion of the image features is shown in the

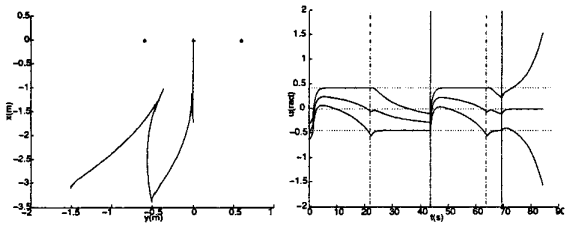

Figure 8: Simulation of image-based switching controller for multiple switches.

right plot of Figure 8. The vertical lines mark places where switches occur. In the first region the controller tracks the left doorway feature to its largest allowable value, until the right feature hits the boundary. Then, the robot reverses and the controller switches to tracking the right-hand feature. Two additional switches occur, until the robot has reached the center region, at which point the centering controller takes over and drives the robot through the doorway.

5 Discussion

We have also designed a user-interface to allow the wheelchair operator to select doorway features [11]. A possible enhancement will be to have the computer preprocess the image to highlight possible doorways to make the selection by the user even easier.

Lastly, we note that the issues arising in doing visual servoing with nonholonomic robots and image-plane constraints lead to some very interesting challenges. We have chosen a switched controller feedback approach that shows a good deal of promise in tackling these general issues. There are parallels to the work of Cowan and Koditschek [3], where navigation functions are used with an omnidirectional robot. Our switched controller provides a potential mechanism for solving this problem in the presence of nonholonomic constraints.

6 Conclusions

We have introduced an interesting new wheelchair system that combines user interaction with intelligent control and multi-sensor feedback. We have presented a control algorithm targeted at solving the doorway navigation problem for a nonholonomically constrained robot. A switched, image-based controller, has been shown to work quite well both in simulation and on our experimental platform. Future experiments will be done in testing the levels of supervised autonomy that can be obtained with a human user.

Acknowledgments

The authors thank Dr. Vijay Kumar for insightful discussions and guidance on this project. We are indebted to both Terry Kientz and Ian Glaser for designing mounts for the laser and cameras. We would also like to acknowledge Ben Backus for deriving the regions of attraction. We gratefully acknowledge support from NSF grant IIS-0083240 and DUE-9979635.

References

[1] S. Hutchinson, G. Hager, and P. Corke, "A tutorial on visual servo control," *IEEE Trans. on Robotics and Automation*, May 1996.

[2] E. Cervera and P. Martinet, "Combining pixel and depth information in image-based visual servoing," in *Proceedings of the 9th International Conference on Advanced Robotics, ICAR*, (Tokyo, Japan), pp. 445–450, October 1999.

[3] N. J. Cowan and D. E. Koditschek, "Planar image based visual servoing as a navigation problem," in *Proc. Int. Conf. Rob. and Automation*, (Detroit, MI), pp. 611–617, May 1999.

[4] P. Martinet and J. Gallice, "Position based visual servoing using a non-linear approach," in *Proc. IEEE/RSJ Int. Conf. Intelligent Robots and Systems*, vol. 1, (Korea), pp. 531–536, October 1999.

[5] Y. Ma, J. Košecká, and S. Sastry, "Vision guided navigation for a nonholonomic mobile robot," *Trans. on Robotics and Automation*, vol. 15(3), pp. 521–536, June 1999.

[6] F. Conticelli, D. Prattichizzo, F. Guidi, and A. Bicchi, "Vision-based dynamic estimation and set-point stabilization of nonholonomic vehicles," in *Proc. IEEE Int. Conf. Robotics and Automation*, (San Francisco, CA), pp. 2771–2776, April 2000.

[7] B. Espiau, F. Chaumette, and P. Rives, "A new approach to visual servoing in robotics," *IEEE Trans. on Robotics and Automation*, vol. 8(3), pp. 313–326, June 1992.

[8] F. Chaumette, "Visual servoing using image features defined upon geometric primitives," in *Proc. 33rd Conf. Decision and Contr.*, (Lake Buena Vista, Florida), pp. 3782–3787, December 1994.

[9] C. Eberst, M. Andersson, and H. Christensen, "Vision-based door-traversal for autonomous mobile robots," in *Proc. IEEE/RSJ Int. Conf. Intelligent Robots and Systems*, (Japan), 2000.

[10] C. Canudas de Wit and O. J. Sørdalen, "Exponential stabilization of mobile robots with nonholonomic constraints," *IEEE Transactions on Automatic Control*, vol. 37(11), pp. 1791–1797, November 1992.

[11] R. S. Rao, K. Conn, S. H. Jung, J. Katupitiya, T. Kientz, V. Kumar, J. Ostrowski, S. Patel, and C. J. Taylor, "Human robot interaction: Applications to smart wheelchairs," in *Proc. IEEE Int. Conf. Robotics and Automation*, (Washington, DC), 2002.